ELSEVIER

Journal of Magnetism and Magnetic Materials 169 (1997) 178–192

Journal of magnetism and magnetic materials

Domain wall pinning sites in $Sm(CoFeCuZr)_x$ magnets

Bunsen Y. Wong[1], Matthew Willard, David E. Laughlin*

Department of Materials Science and Engineering, Carnegie Mellon University, Pittsburgh PA15213, USA

Received 13 September 1996

Abstract

The magnetic domain structure of $Sm(CoFeCuZr)_x$ magnets was studied along various crystallographic zone axes with high resolution Focault mode Lorentz microscopy. The domain wall has been observed to be pinned at (1) 60° hexagonal (H) $SmCo_5$ cell boundaries, (2) features parallel to RSm_2Co_{17} c-axis, (3) features parallel to the RSm_2Co_{17} basal plane, and (4) linear features with no specific crystallographic direction. The wall pinning features which are parallel to the c-axis were determined to be RSm_2Co_{17} antiphase boundaries (APB) and possibly vertical section of $HSmCo_5$ cell boundaries. Both these microstructure features were found to have a higher Cu content than the RSm_2Co_{17} matrix. This chemical inhomogeneity leads to local variations in magnetocrystalline anisotropy which assists domain wall pinning, similar to the role of $HSmCo_5$ suggested previously. Since not all the domain wall pinning features observed are in a strained state, this suggested that chemical segregation to nanostructural features such as $HSmCo_5$ cell boundaries and APB play a more important role than coherency strain in determining H_{ci}.

Keywords: Domain walls; Pinning sites; Antiphase boundaries; Sm(CoFeCuZr) alloy

1. Introduction

Sm-Co permanent magnets have attained commercial importance since their discovery almost three decades ago [1–7]. Their high energy product (BH_{max}) along with their high Curie temperature (T_C) make them unique among the commercially available permanent magnets [8]. The high BH_{max} in this family of precipitation magnets stems primarily from their high intrinsic coercivity (H_{ci}) and its origin has been studied extensively [9–20]. Previous microstructural investigations on Sm–Co magnets have revealed a network of coherent $SmCo_5$ cell boundaries precipitating within the Sm_2Co_{17} matrix (Fig. 1a) [15]. The precipitation reaction is initiated through thermal activation brought about by various metallurgical heat treatments. At the solutionizing temperature (circa 1100°C), Sm_2Co_{17} has an off-stoichiometric disordered hexagonal (H) structure whereas below the transformation temperature, the alloy transforms into an ordered stoichiometric rhombohedral (RSm_2Co_{17}) structure and an ordered hexagonal

* Corresponding author. Tel.: + 1-412-268-2706; fax: + 1-412-268-7169; e-mail: dlop@andrew.cmu.edu.

[1] Now at Hyundai Electronics America, Max Media Division, 2001 Fortune Drive, San Jose, CA 95132, USA.

PII S0304-8853(96)00719-6

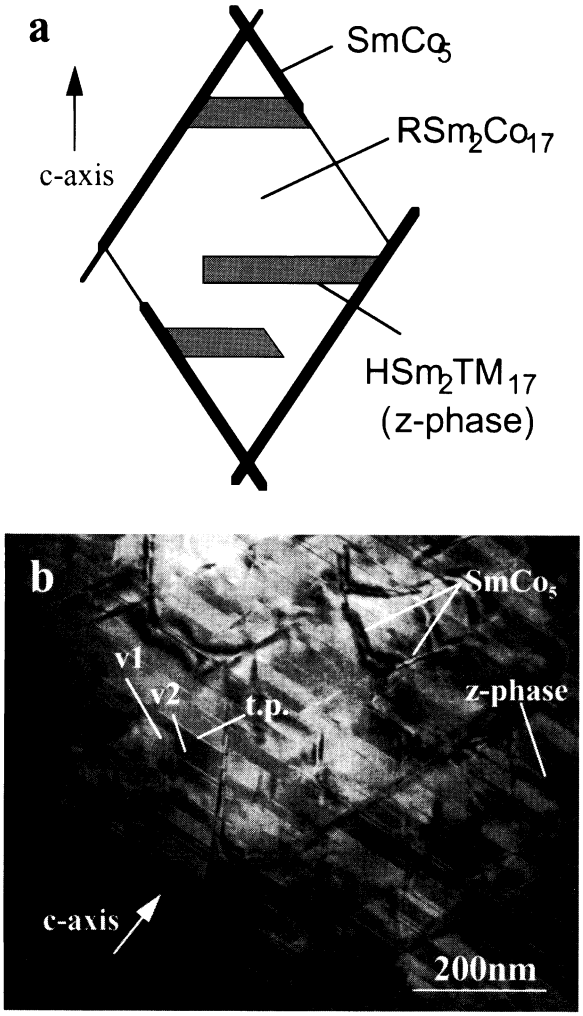

Fig. 1. (a) A schematic of the structure in a Sm_2Co_{17} precipitation magnet. (b) BF image taken along $[\bar{5}\,4\,1\,0]$ RSm_2Co_{17} of a multiphase $Sm(CoFeCuZr)_x$ magnet. The two ordered variants, v1 and v2, are marked along with their twin plane.

(H) $SmCo_5$ phase [21–24]. Both RSm_2Co_{17} and $HSmCo_5$ are based on a hexagonal layer structure which is made up of alternating layers consisting of either Co atoms or a mixture of Co and Sm atoms [25]. The RSm_2Co_{17} phase can be viewed as an ordered crystallographic derivative of $HSmCo_5$. The possible phases present in this system are listed in Table 1. [26, 27]. $HSmCo_5$ is known to precipitate coherently on the $\{0\,1\,\bar{1}\,1\}$ planes of the

Table 1
Common phases found in the $Sm(CoFe)_{5+x}$ system

Comp.	Structure	Symmetry	c/a
$x = 0$	$SmCo_5$	P6/mmm, ordered	0.795
$0 < x < 2$	Sm_2Co_7	P6/mmm, disordered	$0.795 < \cdot < 0.837$
$x = 3.5$	RSm_2Co_{17}	R3m, ordered	$0.837 < \cdot < 0.849$
$3.5 < x < 7$	HSm_2Co_{17}	$P6_3/mmc$, ordered	< 0.85

RSm_2Co_{17} matrix in order to minimize the misfit strain between them [10–15]. This results in rhombic RSm_2Co_{17} cells, lined with $HSmCo_5$ cell boundaries, centered with respect to the RSm_2Co_{17} c-axis. The coherency strain is believed to play an important role in the pinning of domain walls [28–32].

In order to attain the highest H_{ci} in Sm–Co magnets, Fe, Cu and Zr alloying additions are necessary which resulted in a magnet with a composition of $Sm(CoFeCuZr)_x$ ($7.5 \leqslant x \leqslant 8.5$) [33–35]. Fig. 1b shows a typical microstructure of such a multiphase magnet viewed along the $(\bar{5}\,4\,1\,0)$ RSm_2Co_{17} zone axis. The addition of Zr promotes the precipitation of Zr rich hexagonal thin plates (z-phase) on the basal planes in addition to the cellular microstructure. These thin plates are thought to function as diffusion paths for Cu and Fe atoms to segregate to $HSmCo_5$ and RSm_2Co_{17} respectively during isothermal aging [11, 14, 19, 36]. This chemical inhomogeneity causes a corresponding variation in the local magnetocrystalline anisotropy and establishes low energy sites to attract domain walls [37, 38]. Furthermore, microstructural studies have suggested that the magnitude of H_{ci} is very sensitive to the size and density of both the cell boundaries and the z-phase plates.

The orientation relationships between the various phases are well documented [16] and they are listed below:

$$(0\,0\,0\,1)\ HSmCo_5 \parallel (0\,0\,0\,1)\ RSm_2Co_{17} \parallel (0\,0\,0\,1)\ z,$$

$$[1\,1\,\bar{2}\,0]\ HSmCo_5 \parallel [1\,\bar{1}\,0\,0]\ RSm_2Co_{17} \parallel [1\,\bar{1}\,0\,0]z.$$

Effective domain wall pinning sites in magnetic materials must have similar dimensions as the domain wall but contrasting magnetic characteristics [30, 43]. The theoretically calculated wall width for high magnetocrystalline anisotropy Sm–Co magnets is between 1 and 5 nm. Hence, the most effect pinning sites should fall within this size range. It is imperative to determine the nature of such features in order to produce a better magnet.

An important approach to understanding the effect of various microstructural features on the extrinsic magnetic properties is through the use of Lorentz microscopy (LM). Previous studies [19, 29, 39, 40] on $Sm(CoFeCuZr)_x$ magnets have attributed the high H_{ci} to domain wall pinning by the $HSmCo_5$ cell boundaries. The crystalline anisotropy differentiation at cell boundaries caused by the coherency strain and the local chemical fluctuations are thought to be the ground for domain wall pinning. The wavy domain walls observed in Sm–Co magnets substantiates this conclusion. However, such a wavy wall structure has been observed in both high and low coercivity magnets which possess similar microstructure [22, 23, 41, 42]. This indicates the possibility of other microstructural features contributing to the coercivity mechanism.

Recently, we applied a high resolution Focault mode Lorentz microscopy technique [44, 45] to study NiFe domain wall profile [46]. The technique has resolution in the nanometer range and has demonstrated the capacity to resolve fine magnetic and microstructural features simultaneously. Furthermore, one can obtain a selected electron diffraction (SAD) pattern on the area of interest by adjusting the intermediate lens current. As a result, the domain pattern with respect to the orientation and the microstructure can be correlated. In this work, we studied the nature of the pinning sites in $Sm(CoFeCuZr)_x$ magnets. The magnetic domain structure along various crystallographic orientations is studied within the frame work of Lorentz microscopy. In order to identify the characteristics of the pinning sites, the magnet was also studied with conventional transmission electron microscopy (TEM) and electron microprobe analysis for structural and chemical clarification.

2. Experimental procedures

The $Sm(CoFeCuZr)_x$ permanent magnet used in this study was cast by vacuum induction melting. A solution heat treatment to homogenize the magnet was carried out at 1180°C for 7 h and then quenched by argon to room temperature. The sample was then reheated to 846°C for isothermal sintering followed by a slow cool to 400°C for aging. The magnetic properties of the magnets are listed in Table 2 and the demagnetizing curve is shown in Fig. 2a.

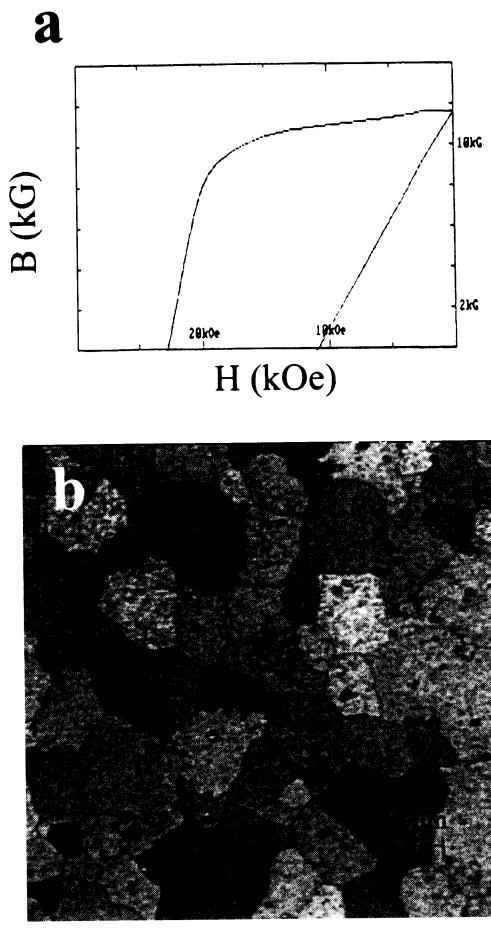

Fig. 2. (a) The demagnetization curve of the $Sm(CoFeCuZr)_x$ magnet studied. (b) Optical micrograph of the $Sm(CoFeCuZr)_x$ magnet showing no sign of chemical inhomogeneity.

Table 2
The measured magnetic properties of the $Sm(CoFeCuZr)_x$ magnet

B_r	11.4 kG
H_{ci}	22.8 kOe
H_k	14.9 kOe
BH_{max}	31.8 MG Oe
Density	8.37 g/cc

Thin sections of the specimen were then sliced along the *c*-axis. TEM specimens were prepared by first punching 3 mm discs from these sections. The discs were then mechanically lapped down to a thickness of 100 μm and then dimpled to a thickness of 10 μm in the middle of the disc. Final thinning was carried out by dual beam ion-milling until the specimen perforates. Focault mode LM studies on the TEM specimens was performed on a JEOL 4000EX microscope with the objective lens switched off. The microscope is equipped with a Gatan image energy filter (GIF) unit which consists of a set of magnetic lenses to provide further magnifying power. The specimen was also studied by conventional TEM on a Philips 420T microscope for microstructural identification. In addition, the local chemical composition was investigated using electron microprobe analysis on a Scanning TEM unit equipped with an Energy Dispersive X-ray (EDX) analyzer. The probe size was 10 nm.

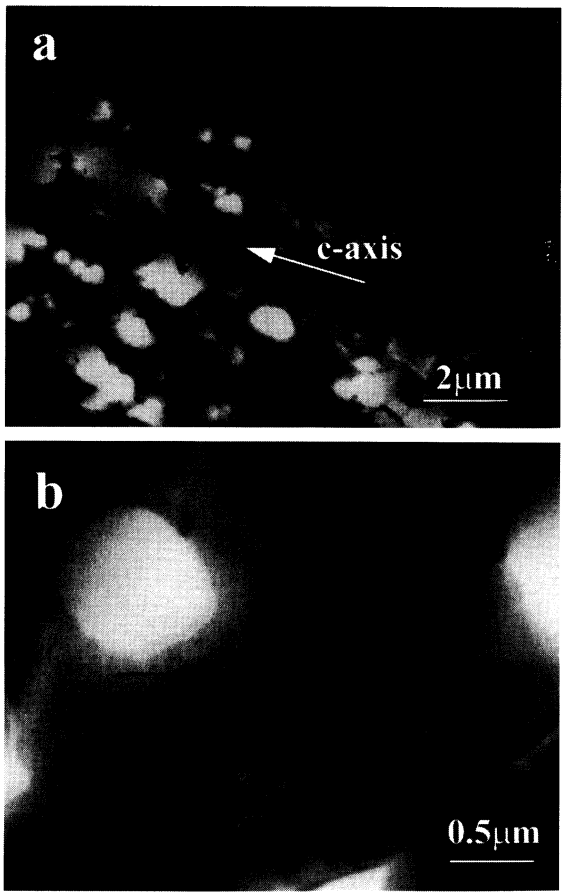

Fig. 3. (a) A low magnification Focault mode Lorentz micrograph showing the antiparallel domains in the $Sm(CoFeCuZr)_x$ magnet. (b) A magnified image showing the wave domain wall profile (black arrow).

3. Results

3.1. Metallography

The optical micrograph of the specimen is shown in Fig. 2b. It shows an average grain size of 50 μm and has no sign of abnormal grain growth. The etch is uniform and shows no detectable second phase such as Sm_2Co_7. The small black circular features in the picture are sintering pores.

3.2. Lorentz microscopy

A low magnification Lorentz micrograph of the domain configuration in the $Sm(CoFeCuZr)_x$ magnet is shown Fig. 3a. The 'fingerlike' or antiparallel stripe domains, similar to what have been previously reported, are present. The magnified image (Fig. 3b) shows a wavy domain wall structure which has been attributed to the pinning of domain walls by $SmCo_5$ cell boundaries discussed above [11–20].

A pair of high resolution Lorentz images taken along an arbitrary zone axis are shown in Fig. 4a and Fig. 4b. The domain contrast reverses itself as the position of the aperture is translated. The corresponding bright field (BF) image is shown in Fig. 4c. No $SmCo_5$ cell boundaries or z-phase can

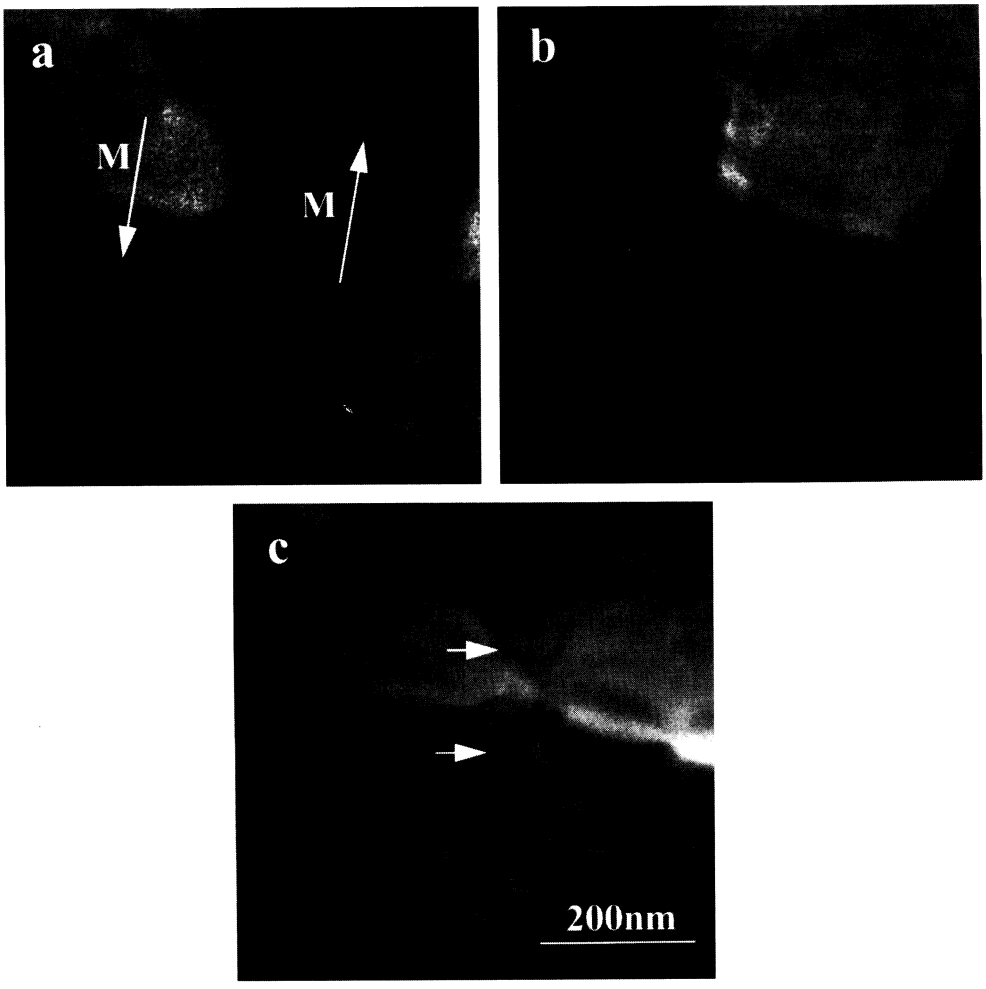

Fig. 4. (a), (b) A pair of magnetic domain images of the $Sm(CoFeCuZr)_x$ magnet observed along an arbitrary zone axis (M: direction of magnetization). (c) Corresponding bright field (BF) image with the white arrows pointing to the boundaries.

be identified from these images because the zone axis of observation is irrational. By comparing these three images, the domain wall appears to lie along the boundaries of certain cell structures (white arrows, Fig. 4c), resulting in a wavy domain wall profile. However, the exact nature of these boundaries cannot be determined from these images. To resolve the pinning sites, it is necessary to study the domain structure along rational zone axes.

Fig. 5a and Fig. 5b show another pair of Lorentz images along with the BF image (Fig. 5c) taken close to the $[1\,\bar{1}\,0\,1]$ RSm_2Co_{17} zone. The $HSmCo_5$ cell boundaries can be identified in all the images whereas the z-phase is still absent because the basal plane is not observed edge-on. A section of the wall is contained by the $HSmCo_5$ cell boundaries whereas the remainder of the wall rests in between the boundaries. From this vantage, the domain wall does not seem to have a preference to lie on cell boundaries

Fig. 6 shows the Lorentz and the BF images observed along the $[\bar{5}\,4\,1\,0]$ zone of RSm_2Co_{17}. Both the $HSmCo_5$ cell boundaries and the thin z-phase plates are visible. The cell boundaries are

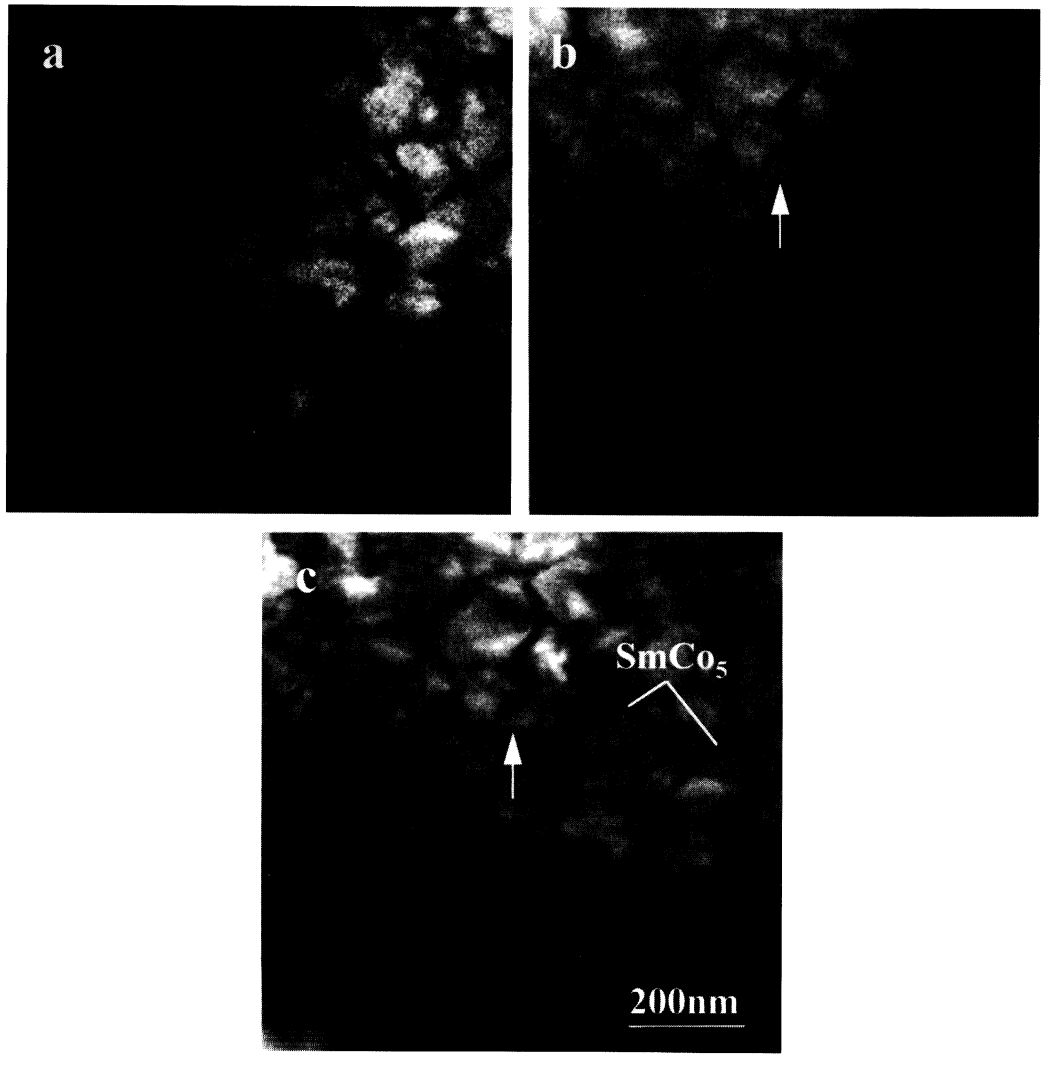

Fig. 5. (a), (b) Magnetic domain images of $Sm(CoFeCuZr)_x$ magnet observed along the [1 0 $\bar{1}$ 1] RSm_2Co_{17} zone axis showing a wavy domain wall. (c) Corresponding bright field (BF) image with the $HSmCo_5$ cell boundaries marked. The white arrows point out the location of the domain wall in the images.

symmetric above the RSm_2Co_{17} c-axis and they make an angle of about 60° with respect to the basal plane. The domain wall is clearly segmented and a portion of it is resting on *white linear features* which are about 80 nm long and are almost perpendicular to the basal plane (white arrows, Fig. 6b). These features are neither Fresnel image of the domain wall nor voids as they remain white during over and under-focusing of the focusing lens. The rest of the domain wall lies parallel to the $HSmCo_5$ cell boundaries indicating that those are pinning sites (black arrow, Fig. 6a). The corresponding SAD pattern from these images is shown in Fig. 7a. Closer inspection of the ($\bar{1}$ $\bar{2}$ 3 2) and ($\bar{1}$ $\bar{2}$ 3 1) RSm_2Co_{17} diffraction spots revealed that they are spilt in to two as a result of the Lorentz deflection caused by the anti-parallel magnetization of the specimen (Fig. 7b).

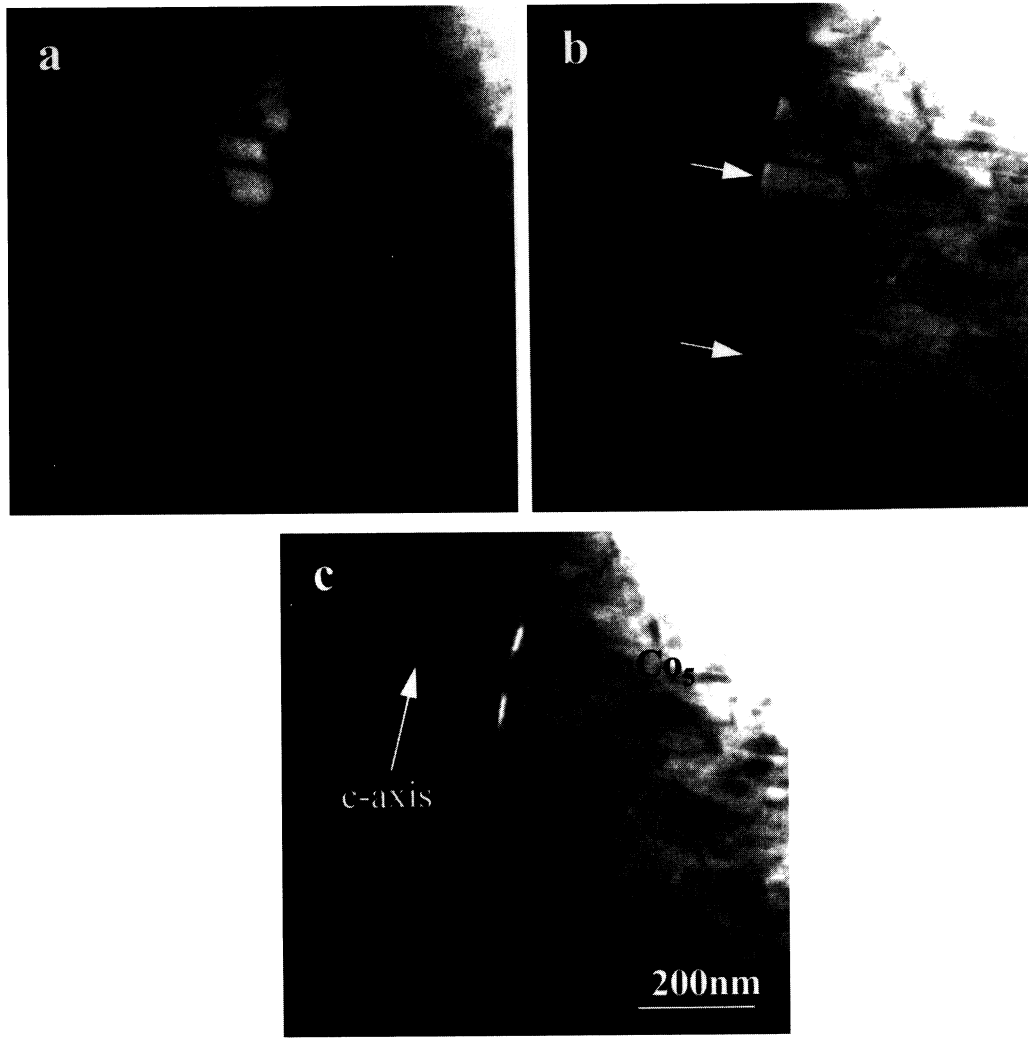

Fig. 6. (a), (b) Lorentz domain images along the RSm_2Co_{17} [$\bar{5}$ 4 1 0] zone axis. The white arrows mark the perpendicular segment of the domain wall whereas the black arrow points to where the wall is pinned by $HSmCo_5$ cell boundaries. (c) Corresponding BF image with the direction of the c-axis marked.

Another set of images taken close to the [$\bar{5}$ 4 1 0] zone axis is shown in Fig. 8. In this situation, most of the wall was found to be pinned at the $HSmCo_5$ cell boundaries. However, a small segment has been found to lie in the basal plane (black arrow, Fig. 10a). This is an unusual observation since the configuration constitutes a high magnetostatic energy situation with the anti-parallel magnetization pointing head on to each other.

Fig. 9a and Fig. 9b show the Lorentz images along the [1 1 $\bar{2}$ 0] RSm_2Co_{17} zone axis. They clearly illustrate a situation in which the domain wall does not come to rest at the $HSmCo_5$ cell boundaries but is parallel to the c-axis. It is pinned by a long white linear feature perpendicular to the basal plane. Similar to what has been seen above, this linear feature is neither a defocused image of the wall nor a void.

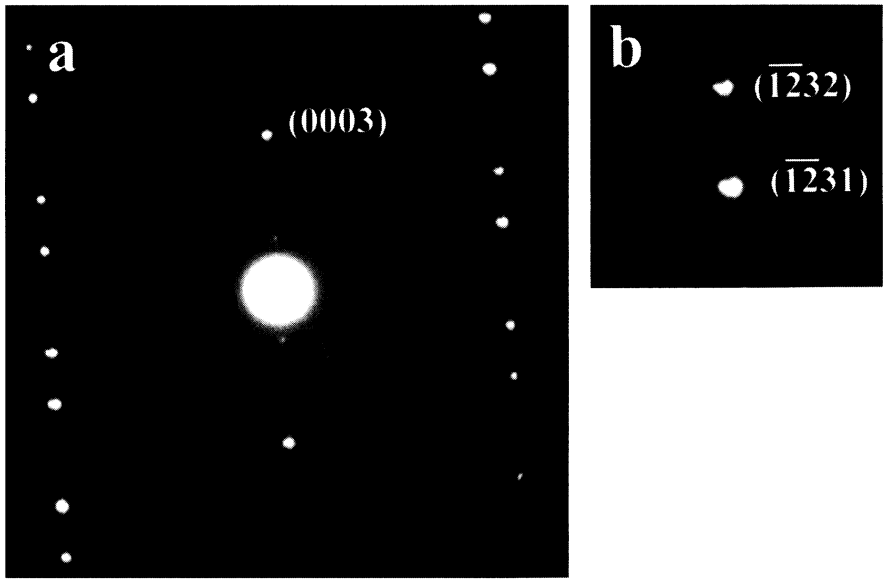

Fig. 7. (a) Selected area diffraction (SAD) pattern of the specimen area shown in Fig. 6. (b) Bifurcation of the ($\bar{1}\,\bar{2}\,3\,1$) and ($\bar{1}\,\bar{2}\,3\,2$) diffraction spots due to the antiparallel domains.

The domain pattern viewed close to [1 0 $\bar{1}$ 0] RSm_2Co_{17} is shown in Fig. 10b. One of the domain walls clearly sits on $HSmCo_5$ since its jaggedness corresponds to the location of the cell boundaries in the BF image. On the other hand, a major portion of the other domain wall lies parallel to the *c*-axis (white arrow). Unfortunately, the feature on which the perpendicular segment of the wall sits cannot be resolved due to thickness contrast. Fig. 11b shows another domain image taken along the same zone axis. In this case, the wall follows the contour of a black linear feature which is in no way associated with the $HSmCo_5$ cell boundaries (white arrow, Fig. 11b). In all the Lorentz images, the z-phase does not seem to play any role in pinning the domain walls.

3.3. Microstructural identification

In order to identify the nature of the pinning sites other than the $HSmCo_5$ cell boundaries, especially those which are parallel to the *c*-axis, the microstructure along various RSm_2Co_{17} zone axes have also been studied. The BF picture taken along [$\bar{5}$ 4 1 0] was shown previously in Fig. 1b. Besides the $HSmCo_5$ cell boundaries and the z-phase plates, no other distinctive feature can be observed. The RSm_2Co_{17} cells are approximately 80 nm in size and the z-phase plates are about 8 nm thick. As seen by the diffraction contrast, there are two RSm_2Co_{17} ordered domain variants, d1 and d2, in the crystal [16]. They formed during quenching from the high temperature HSm_2Co_{17} phase. These variants are related to each other in a twinned orientation and the z-phase is often found at the twin plane. $HSmCo_5$ can be seen to form at some of the antiphase boundaries (APB) between the two ordered domain variants. By tilting the specimen 3° from the [$\bar{5}$ 4 1 0] zone, the contrast between the variants is enhanced (Fig. 12). A number of APBs perpendicular to the basal plane are now clearly visible (Fig. 12a) and in addition, other features parallel to the *c*-axis can also be observed under this imaging condition (black arrow, Fig. 12b).

The BF image along the [1 1 $\bar{2}$ 0] and [1 0 $\bar{1}$ 0] RSm_2Co_{17} zone axes are shown in Fig. 13. No distinctive feature along the *c*-axis can be observed perhaps due to imaging conditions. However, when the specimen is tilted 5° from the [1 1 $\bar{2}$ 0] zone, the contrast of the $HSmCo_5$ cell boundaries become

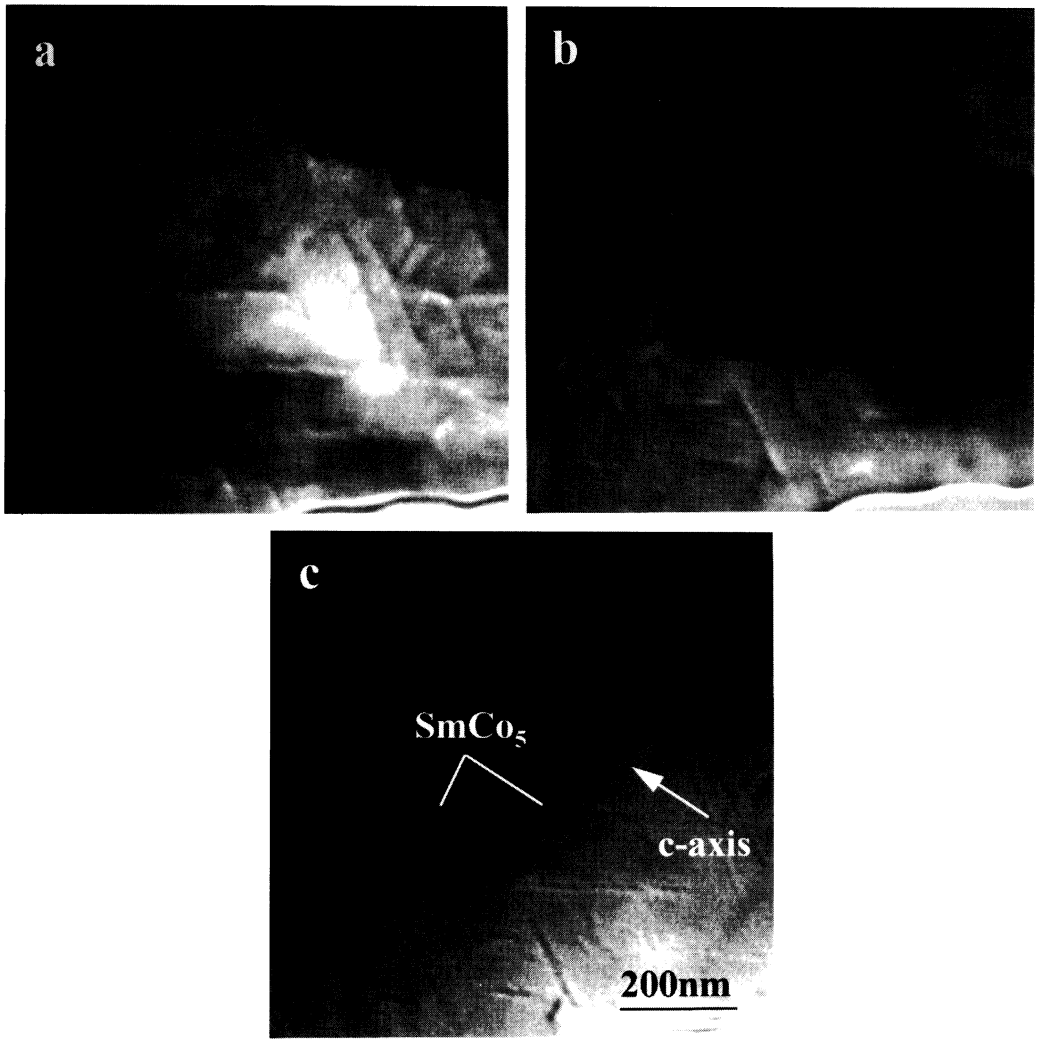

Fig. 8. (a), (b) Domain images of the $Sm(CoFeCuZr)_x$ magnet taken along the RSm_2Co_{17} [$\bar{5}$ 4 1 0] zone axis. The black arrow shows a segment of the domain which lies in the basal plane. (c) Corresponding BF image.

serrated and features perpendicular to the basal plane can be found at the tip of the boundaries (Fig. 14). The modification in the strain state at the tip of the cell boundaries most likely caused this rotation from the normal 60° orientation.

The black linear feature observed by LM studies in Fig. 11 can not be found in our conventional TEM studies. The reason behind this is unclear but such features might have been ion-milled away during specimen cleaning.

3.4. Chemical identification

The chemical compositions of the three main phases have been studied extensively [14, 36]. It has been found that solubility of Cu is small in RSm_2Co_{17} and it partitions to the $HSmCo_5$ cell boundaries. The EDX spectra of the overall composition of the specimen and the RSm_2Co_{17} matrix are shown in Fig. 15a and Fig. 15b. There is a clear deficiency of Cu in the matrix. The composition

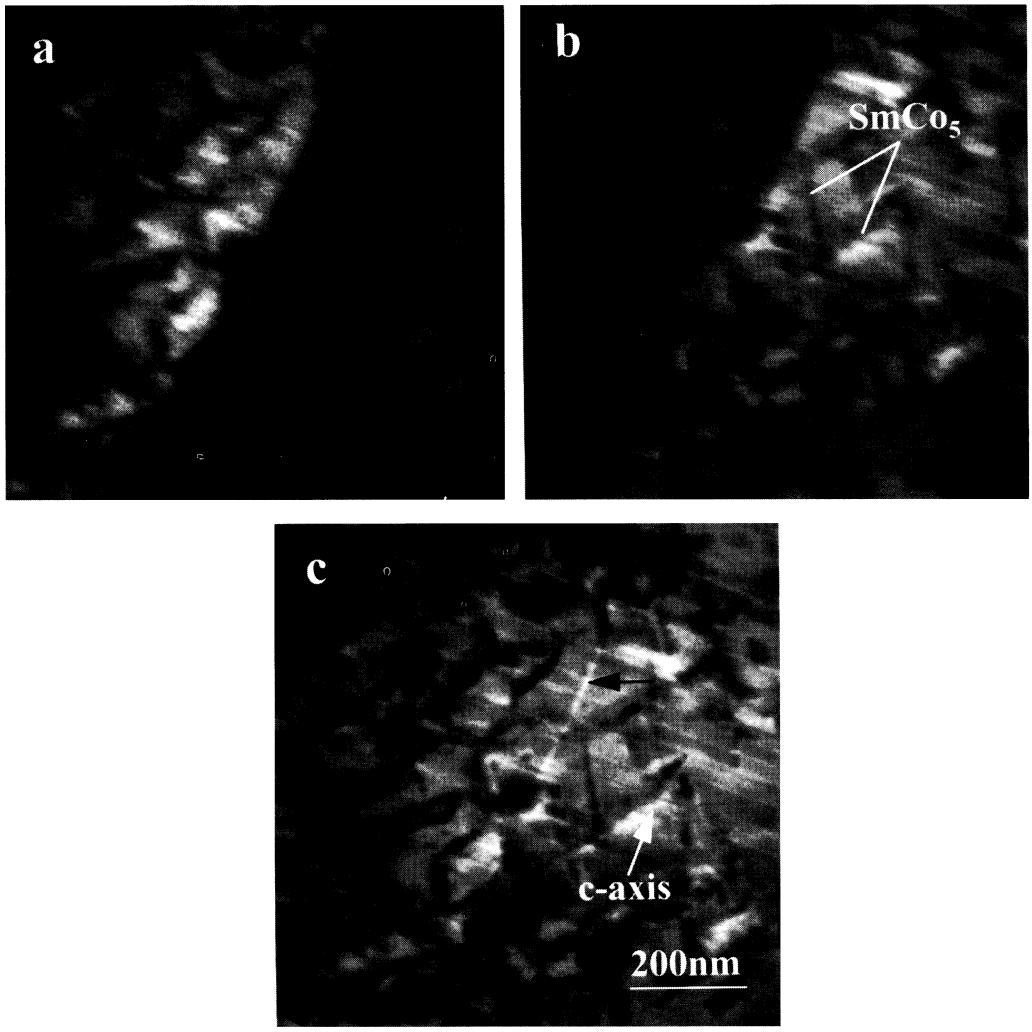

Fig. 9. (a), (b) Lorentz domain images of $Sm(CoFeCuZr)_x$ magnet along [1 1 $\bar{2}$ 0] RSm_2Co_{17}. The domain wall comes to rest at a linear white feature (black arrow) parallel to the *c*-axis. (c) Corresponding BF image.

at the vertical APB and that at the straight section of the $HSmCo_5$ cell boundaries are shown in Fig. 15c and Fig. 15d, respectively. Although situated within the matrix between the two variants, the APB does have a higher Cu content than RSm_2Co_{17}. The vertical section of $HSmCo_5$ has a higher Cu content than the matrix even though it is not oriented like the normal cell boundaries.

4. Discussion

From the results of LM studies there are four locations in which the domain wall has been observed to be pinned: (a) at 60° with respect to the basal plane, (b) parallel to the *c*-axis, (c) along the basal plane and (d), a long linear feature which has no preferential orientation. The first category belongs to the $HSmCo_5$ cell boundaries and the

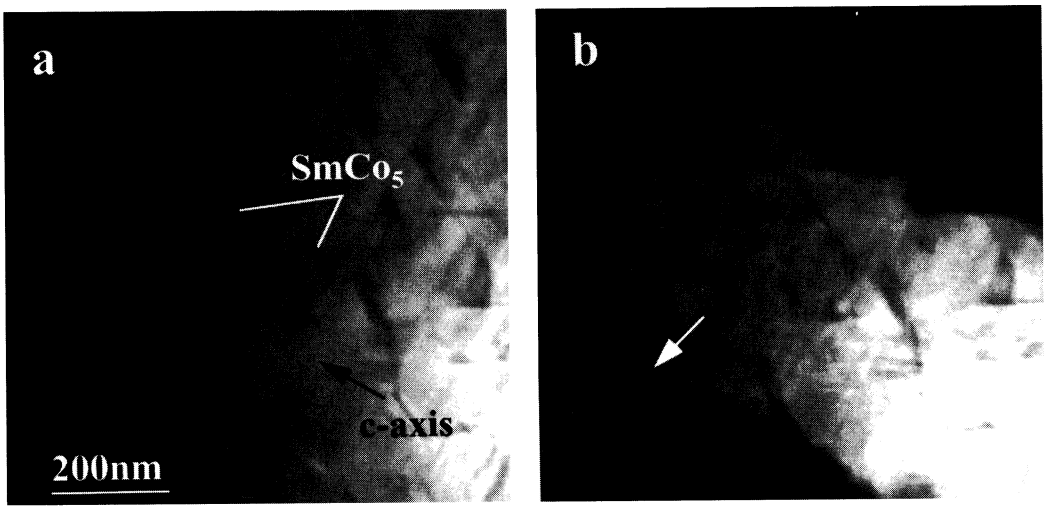

Fig. 10. (a) BF and (b) Lorentz images taken along [1 0 $\bar{1}$ 0] RSm_2Co_{17}. The top domain wall lies along the $HSmCo_5$ cell boundaries giving it its wavy character. However, some section of the bottom domain wall lies parallel to the c-axis.

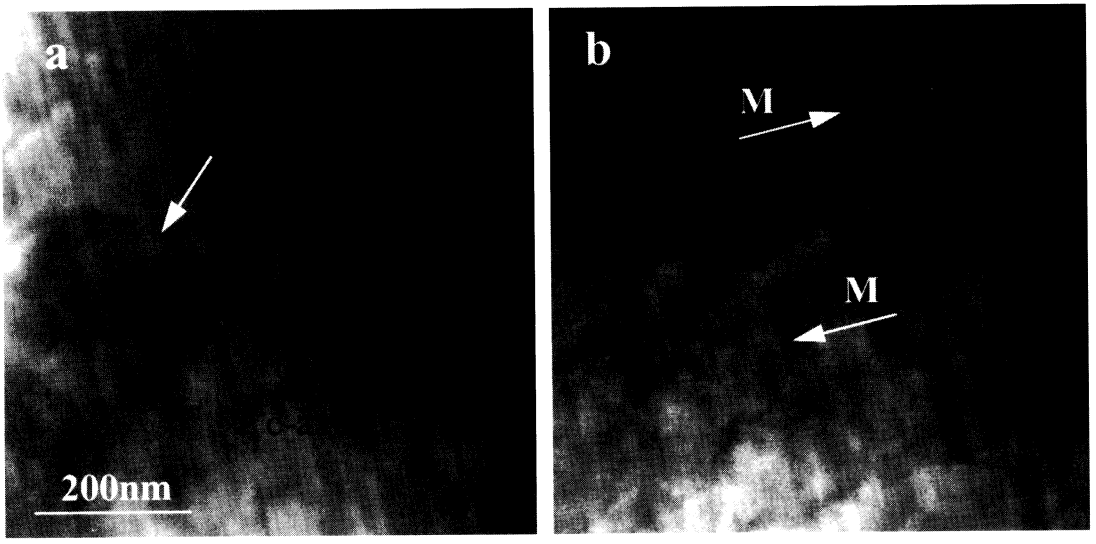

Fig. 11. (a) BF and (b) Lorentz images taken near [1 0 $\bar{1}$ 0] RSm_2Co_{17} and near a grain boundary. The boundary does not have an effect on the domain wall location because of its orientation.

reason behind their pinning effect has been discussed extensively [9–16, 29–31]. From the microstructural investigations, there are two types of features which are parallel to the c-axis. First is the RSm_2Co_{17} APB and the other being the rotated tip of the $HSmCo_5$ cell boundaries. By comparing their dimensions, it appears that the APBs are closer to the scale of the pinning features observed in the LM studies. Electron microprobe analysis results have revealed that the Cu content at both microstructural features is higher than the RSm_2Co_{17} matrix which make them viable candidates as attractive pinning sites for domain walls. The reason for Cu enrichment in both cases is

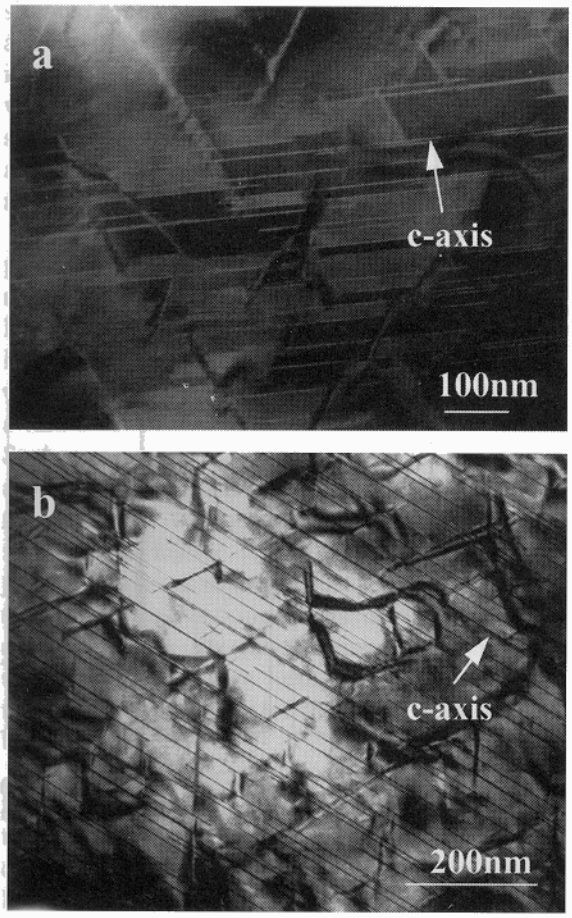

Fig. 12. (a), (b) BF images at 3° from the $[\bar{5}\,4\,1\,0]$ RSm_2Co_{17} zone. APB boundaries between the two RSm_2Co_{17} variants marked by arrows.

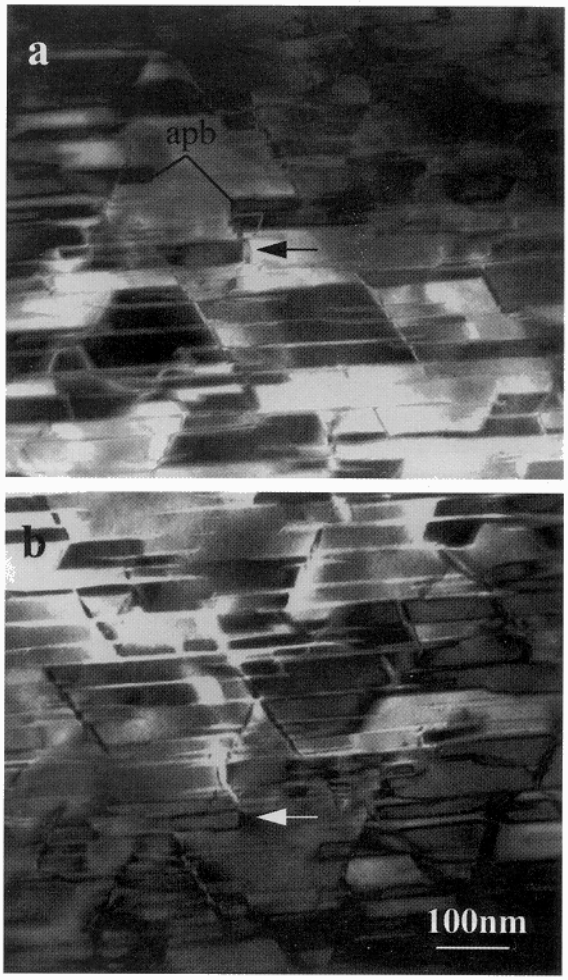

Fig. 13. BF images along (a) $[1\,1\,\bar{2}\,0]$ and (b) $[1\,0\,\bar{1}\,0]$ RSm_2Co_{17}. The microstructure is similar to Fig. 1b.

similar to that behind the 60° cell boundaries. To understand the origin of this chemical inhomogeneity and its possible effect on the magnetic properties, the transformation reaction has to be considered. The reaction sequence can be generalized as follows [22, 23]:

$$HSm_2Co_{17} \xrightarrow{\text{quenching}} \text{disordered } RSm_2Co_{17} + \text{residual } HSm_2Co_{17}$$

$$\xrightarrow{\text{isothermal aging}} \text{ordered } RSm_2Co_{17} + HSmCo_5 + \text{z-phase}.$$

At 1180°C, the alloy is homogenized to form the high temperature non-stoichiometric hexagonal HSm_2Co_{17} phase. Upon quenching, the supersaturated solution began to decompose and formed disordered RSm_2Co_{17}. The $H \rightarrow RSm_2Co_{17}$ is a first order allotropic transformation but the exact mechanism for this reaction is still under debate [13, 16, 21, 22, 27]. Residual HSm_2Co_{17} could be found within the solid solution after quench. During isothermal aging, the transformation resulted in two twin-related variants of RSm_2Co_{17} separated by a twin basal plane. In addition, the ordering of

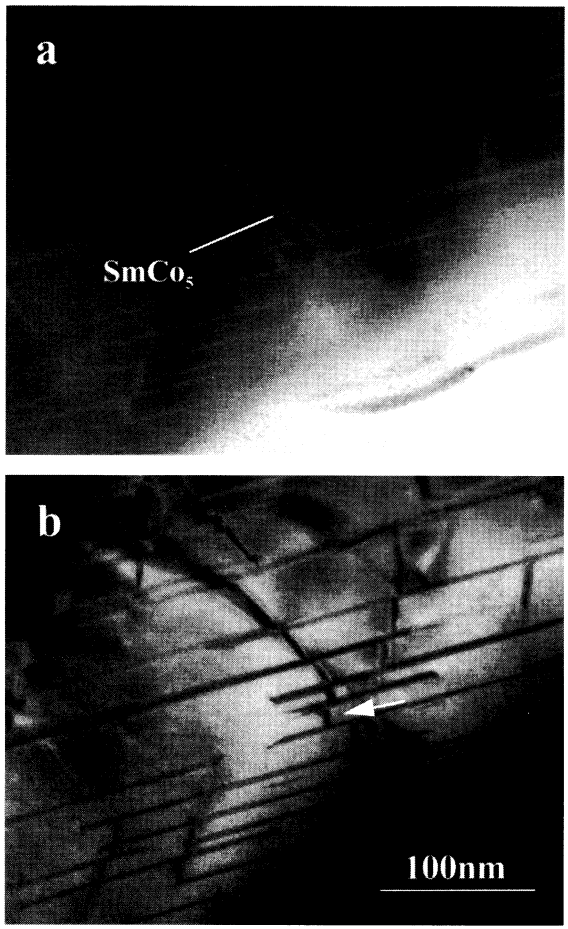

Fig. 14. (a) BF and (b) DF image of the $Sm(CoFeCuZr)_x$ magnet tilted 5° away from the [1 1 $\bar{2}$ 0] zone. The tip of the $HSmCo_5$ cell boundaries (white arrow) has rotated to an orientation parallel to the *c*-axis.

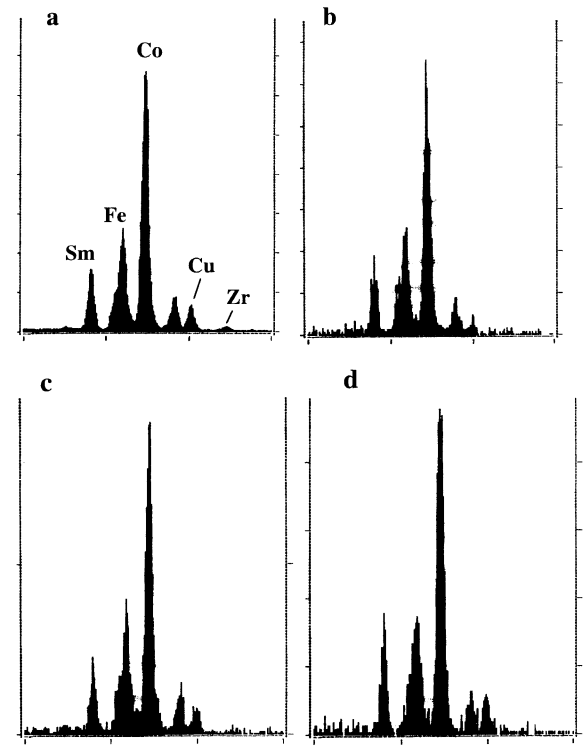

Fig. 15. EDS spectra of (a) $Sm(CoFeCuZr)_x$ magnet, (b) RSm_2Co_{17} matrix, (c) RSm_2Co_{17} APB and, (d) vertical section of the $HSmCo_5$ cell boundaries.

RSm_2Co_{17} begins to proceed. The difference in solubility between HSm_2Co_{17} and RSm_2Co_{17} leads to the redistribution of chemical species. Excess Sm and Cu is repelled from the supersaturated RSm_2Co_{17} to its growing interface by means of diffusion and eventually settles at the boundaries where different growing regions of RSm_2Co_{17} meet. Depending on the relative atomic arrangement, these boundaries can either be a thin region saturated with Sm and Cu metals within the matrix or an APB if the ordering sequence of the different regions does not match. Consequently, $HSmCo_5$ forms to accommodate the excess Sm at these boundaries. However, if the Sm concentration is not in excess at the boundaries, $HSmCo_5$ will not form but only a Cu rich layer or APB remains. It is reasonable to expect the APB to absorb heterogeneity and cause modification in local magnetic anisotropy. The ejection of Zr from RSm_2Co_{17} helps to form the z-phase at this stage. During the slow cooling and prolonged aging at 400°C, the solubility for different chemical species within the stoichiometric matrix decreases and leads to further partitioning of transition metals species to either $HSmCo_5$, z-phase and APB which further enhances the anisotropy variations within the system and strengthen the pinning strength.

Since the magnetization lies along the *c*-axis, the most effective pinning sites are those perpendicular to the basal plane as the area of domain wall is minimized. Hence, the cell boundaries are not

situated at the most effective orientation as they lie at 30° with respect to the *c*-axis. On the other hand, it is entirely logical to assume the APB and the vertical $HSmCo_5$ boundaries to be strong pinning sites as they are parallel to the *c*-axis and have a different chemical content with respect to the matrix.

Chemical inhomogeneity may be behind the surprising observation of heads on antiparallel domains separated by features on the basal plane. RSm_2Co_{17} has a stacking sequence of ABCABCA. However, any microtwins and mistake in stacking will create a stacking fault which is essentially a thin layer of hexagonal phase within the matrix. Such microtwins have been observed readily by atomic resolution TEM [19]. Since the solubility of Cu and other transition metals in the hexagonal structure is higher than in the rhombohederal phase, it is reasonable to expect segregation of such species to the stacking faults during isothermal aging. However, the composition of non-magnetic species in such a thin hexagonal region must be relatively high in order for the wall to lie parallel to the basal plane.

The long linear feature cannot be exactly identified as it has no preferred crystallographic orientation. However, it, alone with other observed domain wall pinning features, raises the point that $HSmCo_5$ cell boundaries alone are not responsible for domain wall pinning. Since, most of such features have no coherency strain associated with them, it suggests that strain is not as important as chemical inhomogeneity in controlling H_{ci}. The observation from this work indicates that local segregation of chemical species to microstructural features with the *appropriate dimension*, such as $HSmCo_5$ cell boundaries and APB, etc. can most effectively vary the local magnetic anisotropy thus trapping domain walls and raising H_{ci} [37, 38]. The pinning strength of the various microstructural features is yet to be clarified and in situ reversal experiment is currently under way to clarify this.

5. Conclusions

High resolution LM studies have shown that the RSm_2Co_{17} domain walls were pinned at the following locations:

- 60° $HSmCo_5$ cell boundaries;
- microstructural features parallel to RSm_2Co_{17} *c*-axis;
- RSm_2Co_{17} basal plane;
- long linear features with no specific crystallographic direction.

From the microstructural investigations, the feature which lies along the *c*-axes were determined to be either APB between RSm_2Co_{17} ordered domains or a vertical section of $HSmCo_5$ situated at the tip of the cell boundaries. They were both found to have a higher Cu content than the matrix which makes them effective domain wall pinning sites. The basal plane feature which is responsible for the observation is probably stacking faults saturated with transition metals. Our results suggest that magnetocrystalline anisotropy variation caused by local chemical segregation to features with applicable dimension plays a more important role than coherency strain-induced magnetostriction anisotropy in pinning domain walls.

Acknowledgements

The authors would like to thank Dr. Bao Min Ma for his careful review of the manuscript and insightful discussions. The magnets used in this work were provided by Rhône-Poulenc Basic Chemicals Co. BYW and DEL acknowledge the financial support of Hitachi Metals Ltd. MW and DEL were partially supported by the Air Force Office of Scientific Research, Air Force Material Command, USAF, under grant number F49620-96-1-0454.

References

[1] G. Hoffer and K. Strnat, IEEE Trans. Magn. 2 (1966) 487.
[2] E.A. Nesbitt, J. Appl. Phys. 40 (1969) 1259.
[3] E.A. Nesbitt and J.H. Wernick, Rare Earth Permanent Magnets (Academic Press, New York, 1973).
[4] Y. Tawara and K. Strnat, IEEE Trans. Magn. 12 (1976) 954.
[5] T. Ojima, S. Tomizawa, T. Yoneyama and T. Hori, IEEE Trans. Magn. 13 (1977) 1317.
[6] R.W. Lee, J. Appl. Phys. 52 (1981) 2549.

[7] M.Q. Huang, Y. Zheng and W.E. Wallace, J. Appl. Phys. 75 (1994) 6280.
[8] P. Campbell, Permanent Magnets Materials and Their Applications (Cambridge University Press, Cambridge, 1994).
[9] J.D. Livingston, J. Appl. Phys. 46 (1975) 5259.
[10] J.D. Livingston and D.L. Martin, J. Appl. Phys. 48 (1977) 1350.
[11] R. Mishra and G. Thomas, J. Appl. Phys. 49 (1978) 2067.
[12] T. Yoneyama, S. Tomizawa, T. Hori and T. Ojima Proc. III Int. Workshop on Re–Co Magnets, University of California, San Diego, CA (1978) p. 406.
[13] R.K. Mirsha, G. Thomas, T. Yoneyama, A. Fukuno and T. Ojima, J. Appl. Phys. 52 (1981) 2517.
[14] G.C. Hadjipanayis, E.J. Yadlowsky and S.H. Wollins, J. Appl. Phys. 53 (1982) 2386.
[15] J. Fiedler and P. Skalicky, J. Magn. Magn. Mater. 27 (1982) 127.
[16] L. Rabenberg, R.K. Mishra and G. Thomas, J. Appl. Phys. 53 (1982) 2389.
[17] G.C. Hadjipanayis, J. Appl. Phys. 55 (1982) 2091.
[18] J. Fiedler, P. Skalicky and F. Rothwarf, IEEE Trans. Magn. 19 (1983) 2041.
[19] J. Fiedler, J. Bernardi and P. Skalicky, Mat. Res. Soc. Symp. Proc. 96 (1987) 181.
[20] J. Fiedler, J. Bernardi, K. Ohashi and Y. Tawara, IEEE Trans. Magn. 26 (1990) 1385.
[21] A.E. Ray, IEEE Trans. Magn. 20 (1984) 1614.
[22] A.E. Ray, J. Appl. Phys. 55 (1984) 2094.
[23] A.E. Ray, W.A. Soffa, J.R. Blachere and B. Zhang, IEEE Trans. Magn. 23 (1987) 2711.
[24] F.J. Cadieu, T.D. Cheung and L. Widkramasekara, J. Appl. Phys. 57 (1985) 4161.
[25] W. Ervens, Goldschmidt informiert 48 (1979) 3.
[26] Y. Khan, Phys. Stat. Sol. A 21 (1974) 69.
[27] A.E. Ray, Soft and Hard Magnetic Materials with Applications, ASM Symp. Proc. (ASM, Metals Park, OH, 1986).
[28] H. Nagel, J. Appl. Phys. 50 (1979) 1026.
[29] J. Fiedler, J. Magn. Magn. Mater. 30 (1982) 58.
[30] K.D. Durst, H. Kronmuller and W. Ervens, Phys. Stat. Sol. A 108 (1988) 705.
[31] D. Givord, M.F. Rossignol, D.W. Taylor and A.E. Ray, J. Magn. Magn. Mater. 104 (1992) 1126.
[32] A. Kainvash and I.R. Harris, J. Mater. Sci. Lett. 3 (1984) 18.
[33] Y. Tawara and H. Senno, Jpn. J. Appl. Phys. 12 (1973) 761.
[34] T. Ojima, S. Tomizawa, T. Yoneyama and T. Hori, Jpn. J. Appl. Phys. 16 (1977) 671.
[35] R.L. Bergner, H.A. Leupold, J.T. Breslin, J.R. Shappirio, A. Tauber and F. Rothwarf, J. Appl. Phys. 50 (1979) 2352.
[36] B. Zhang, J.R. Blachere, W.A. Soffa and A.E. Ray, J. Appl. Phys. 64 (1988) 5739.
[37] V.I. Khrabrov, Ya.S. Shur, A.G. Popov and V.S. Gaviko, Phys. Met. Metallogr. (USSR) 59 (1985) 39.
[38] T. Mukai and T. Fujimoto, J. Appl. Phys. 64 (1988) 5977.
[39] G.C. Hadjipanayis, R.C. Hazelton, K.R. Lawless and L.S. Horton, IEEE Trans. Magn. 18 (1982) 1460.
[40] D. Li and K.J. Strnat, J. Appl. Phys. 55 (1984) 2103.
[41] K.N. Melton and R.S. Perkins, J. Appl. Phys. 47 (1976) 2671.
[42] K.N. Melton and H. Nagel, J. Appl. Phys. 50 (1977) 1026.
[43] H. Hoffman, IEEE Trans. Magn. 9 (1973) 17.
[44] N.T. Nuhfer, J. Dooley and M. De Graef, JMSA Proc.: Microscopy and Microanalysis, Kansas City, Missouri (1995) p. 306.
[45] J. Dooley and M. De Graef, Mat. Res. Soc. Symp. Proc. 360 (1995) 189.
[46] B.Y. Wong and D.E. Laughlin, J. Appl. Phys. 79 (1996) 6455.